NIST Technical Note
NIST TN 2380

Thermo-hydrogen refinement and precipitation hardening of laser powder bed fusion Ti-6Al-4V

Nicholas Derimow
Brady G. Butler
Zachary S. Levin
Jake T. Benzing
Joshua Cline
Nik Hrabe

This publication is available free of charge from:
https://doi.org/10.6028/NIST.TN.2380

NATIONAL INSTITUTE OF STANDARDS AND TECHNOLOGY
U.S. DEPARTMENT OF COMMERCE

NIST Technical Note
NIST TN 2380

Thermo-hydrogen refinement and precipitation hardening of laser powder bed fusion Ti-6Al-4V

Nicholas Derimow
Applied Chemicals and Materials Division
Department of Physics
University of Colorado, Boulder, CO 80309

Brady G. Butler
DEVCOM – Army Research Laboratory
ARL South at Texas A&M University, College Station, TX, 77843, USA

Zachary S. Levin
MST-16
Los Alamos National Laboratory, Los Alamos, NM, 87545, USA

Jake T. Benzing
Nik Hrabe
Applied Chemicals and Materials Division
Material Measurement Laboratory

Joshua Cline
Department of Materials Science and Engineering
Texas A&M University, College Station, TX, 77843

This publication is available free of charge from:
https://doi.org/10.6028/NIST.TN.2380

July 2026

U.S. Department of Commerce
Howard Lutnick, Secretary

National Institute of Standards and Technology
Arvind Raman, NIST Director and Under Secretary of Commerce for Standards and Technology

Publication History
Approved by the NIST Editorial Review Board on 2026-01-30

How to cite this NIST Technical Series Publication:
Derimow, N., Butler B. G., Levin, Z. S., Benzing, J. T., Cline, J., Hrabe, N. (2026) Thermo-hydrogen refinement and precipitation hardening of laser powder bed fusion Ti-6Al-4V. (National Institute of Standards and Technology, Gaithersburg, MD), NIST TN 2380. https://doi.org/10.6028/NIST.TN.2380

Author ORCID iDs
Nicholas Derimow: 0000-0001-7526-1836
Brady G. Butler: 0000-0002-7677-9685
Zachary S. Levin: 0000-0003-0704-5538
Jake T. Benzing: 0000-0002-7266-870X
Joshua Cline: 0009-0007-6140-0234
Nik Hrabe: 0000-0001-7585-0980

Contact Information
nicholas.derimow@nist.gov

Submit Comments
nicholas.derimow@nist.gov
325 Broadway
Mail Stop 647
Boulder, Colorado 80305

Abstract

This work investigates the efficacy of solution treatment and over-aging (STOA) as a post-processing step to improve the mechanical properties of laser powder bed fusion (PBF-L) Ti-6Al-4V that has been subjected to a thermo-hydrogen refinement of microstructure (THRM) treatment. THRM was used to promote ductility and globularization of the PBF-L Ti-6Al-4V microstructure, whereas STOA was leveraged to increase the strength through precipitation hardening from coherent Ti_3Al particles within the α phase, known as the α_2 phase. An increase in hardness across the α phase was measured via nanoindentation, and a small increase in strength was measured as a result of over-aging via quasi-static tensile testing, with no loss of ductility. Both of these occurrences are consistent with previous studies of Ti_3Al precipitation leading to increased strength without loss of ductility.

Keywords

Additive Manufacturing; PBF-L; Hydrogen Treatment; Precipitation Hardening.

Table of Contents

List of Tables

List of Figures

1. Introduction

The field of metal additive manufacturing (AM) may at first glance appear to be new, however, it is built upon a foundational understanding of powder metallurgy, rapid solidification, welding, materials processing, and product manufacturing. This amalgamation of fields has provided a basis for the three-dimensional freedom that metal AM provides to the manufacturing sector. That said, the continued integration of historical understanding with new and developing techniques is an ongoing process (e.g., Ti-6Al-4V). The physical metallurgy of Ti-6Al-4V is well understood [1], with typical solidification microstructures consisting of a lamellar $\alpha+\beta$ morphology, where the hexagonal close packed (HCP) α is the predominant, lamellar phase trapping the residual body centered cubic (BCC) β phase between the laths.

Lamellar microstructures, particularly in the case of the primarily HCP Ti-6Al-4V, can present engineering challenges during plastic deformation, as there are fewer degrees of freedom for dislocation slip, as Ti-6Al-4V has preferred slip systems [2–4]. Depending on the cooling rate during Ti-6Al-4V solidification, the initial phase field that is entered is the β phase, which first precipitates α along the prior (parent)-β grain boundaries, followed by the lamellar α that grows into the parent-β grains in accordance with the Burgers orientation relationship [5]. This *grain boundary* α (α_{GB}) is deleterious to the mechanical properties of Ti-6Al-4V, as these features are large pathways/lengths for dislocation slip [6], which is also exacerbated by the parent-β grain size that results in elongated/parallel colonies of $\alpha+\beta$ aligned across the entire region of the parent-β grain during cooling [1]. High cooling rates ($>$ 400 °C /s) can lead to the suppression of the deleterious α_{GB} [7]; however, this results in a super-saturated solid solution of β -stabilizers that are essentially trapped in the room-temperature stable α phase. This resultant super-saturated α is embrittled, and acicular in morphological appearance, thus leading to the metallurgical community referring to this microstructure as a martensite (α'). In metal AM, particularly laser powder bed fusion (PBF-L), the α' microstructure is typically the predominant as-built microstructure due to the high cooling rates inherent to solidification resulting from laser melting [8], and needs to be subjected to heat treatments to decompose the supersaturated α' into a stable $\alpha+\beta$ microstructure [9, 10].

Traditional hot-working techniques have been able to both reduce the effect of the interconnected α_{GB} , as well as transform the lamellar $\alpha+\beta$ microstructure into a more or less equiaxed/globular granular microstructure [11], which is desirable for enhanced fatigue performance of Ti-6Al-4V [12]. However, from an AM perspective, hot-working Ti-6Al-4V is typically not a viable option, as one of the primary functions of AM is to produce net or near-net shape parts. This results in a limitation of available post-process options that do not significantly alter the net shape of the material. Work by Paramore et al. [13] in the powder metallurgical field of Ti-6Al-4V, aimed at preserving the macroscale near-net shape of the part while globularizing the microstructure, has led to the development of heat treatments that leverage a gaseous hydrogen environment. This process is referred to as *thermo-hydrogen refinement of microstructure*, or THRM, to lower the β -transus temperature (from approximately 1000 °C to 825 °C) and allow for a globularization of the microstructure and the introduction and removal of hydrogen during heat treatment processing. As alluded to earlier, the implementation of processing techniques to metal AM is an active area of investigation, with THRM being recently applied to PBF-L Ti-6Al-4V by Knezevic et al. [14], along with work by Dunstan et al. towards parameter optimization tailored for PBF-L Ti-6Al-4V to promote globularization and enhance ductility [15].

In a parallel thrust to enhance the mechanical properties of Ti-6Al-4V, early studies have shown that aging Ti-6Al-4V in the 500 °C to 550 °C range [16, 17] (the α /(α + α_2) solvus [18]) for approximately 100 hours leads to the precipitation of intermetallic Ti_3Al particles (α_2), which are coherent within the α phase of the $\alpha + \beta$ microstructure. These *solution treatment and over-aging* (STOA) processes have been historically leveraged in some of the aforementioned work, essentially as 'standard practice' for achieving optimal properties [1], as the presence of these Ti_3Al particles increase the strength in Ti-6Al-4V with minimal to no loss of ductility [19, 20]. Recent studies of PBF-L Ti-6Al-4V have shown that over-aging treatment can be successfully applied [21], with recent work by Derimow et al. [22], who conducted an analogous *solution treatment and over-aging* of PBF-L Ti-6Al-4V through hot isostatic pressing (HIP) at 920 °C for 2 hours, followed by over-aging at 545 °C in a vacuum furnace for 100 hours. It was observed that there was an approximate increase of 60 MPa in yield strength and 40 MPa in ultimate tensile strength with no loss of ductility. The precipitation hardening was confirmed by Derimow et al. [22] via atom probe tomography (APT), consistent with previous Ti_3Al precipitate characterization in Ti-alloys via APT [23, 24]

The present investigation builds off of previous works by Derimow et al. [22] and Dunstan et al. [15], in which the optimized THRM and globularization routine was implemented with an over-aging step for post-processing to leverage both techniques to potentially improve the mechanical properties of PBF-L Ti-6Al-4V.

2. Methods

Laser powder-bed fusion was carried out externally at an ISO 13485 [25] certified medical device manufacturer. The build details are presented in Table 1. The build utilized plasma atomized powder with nominal oxygen concentration of 0.104 wt.% O measured (via inert gas fusion) prior to the build in the industrial work-flow setting. The build consisted of identical cuboid blocks that were then grouped and subjected to the separate heat treatments in order to maintain a constant chemistry. The blocks were leftover/extra blocks from previous studies conducted by Derimow et al. [26, 27], and were used in the present investigation from the as-built state prior to heat treatment processing.

The chemistry measurements were carried out externally at a Nadcap and A2LA ISO/IEC 17025 [28] accredited laboratory. The chemical content for the as-built blocks was mea-

Table 1. Build parameters for the Ti-6Al-4V specimens in this study.

Parameters	Information
Fabrication	PBF-L
Machine	3D Systems DMP Flex 350[1]
Laser Type	Fiber, 500 W /1070 nm
Software version	DMP Suite v39.1.1
Scan speed	1250 mm/s
Power	245 W
Layer thickness	60 μm
Atmosphere	Argon (Ar)
Pressure	150 mbar
Chamber O_2	$<$ 10 ppm
Feedstock PSD	10 μm – 45 μm
D50	33 μm

sured, except for trace elements. Aluminum, vanadium, and iron were measured by inductively coupled plasma mass spectrometry (ICP-MS) per ASTM E2823-17 [29]. Oxygen and nitrogen were measured per ASTM E1409-13 [30], and hydrogen per ASTM E1447-09 [31], all by inert gas fusion. Carbon was measured by the combustion method (ASTM E1941-10 [32]).

Table 2. Chemical composition in weight %. The ASTM standard specification maximum limits for PBF Ti-6Al-4V Grade 23 (ASTM F3001 [33]) are also indicated. Note, trace elements were not measured.

Element	Grade 23	This build
Al	5.5$<$x$<$6.50	6.48
V	3.5$<$x$<$4.5	4.1
Fe	0.25	0.22
O	0.13	0.13
C	0.08	0.01
N	0.05	0.02
H	0.012	0.009

The heat treatments in this work follow the optimized condition presented by Dunstan et al. [15], where the nomenclature used in this work is such that Ti$|_{\mathrm{H_2+G1}}$ refers to the '850 °C THRM + Globularization' treatment from Dunstan et al., nominally plotted in Fig. 1a, where 850 °C was carried out for one hour in an Ar/H_2 environment, followed by 650 °C for four hours, after which Ar/H_2 was purged from the chamber followed by a vacuum heat treatment at 750 °C for 12 hours. The globularization portion consisted of 950 °C for one hour, and 550 °C for 6 hours. Given the closeness in temperature to the 545 °C over-aging temperature used by Derimow et al. [22], the 550 °C hold was extended to 100 hours (Fig. 1b), to be consistent with the aging time from that work to promote α_2 precipitation.

Microscopy specimens were hot mounted in conductive bakelite and were ground with 320, 400, 600, 800, and 1200 grit SiC paper (U.S. Industrial Grit), polished with 1 μm diamond slurry, and vibratory polished in 50 nm colloidal silica for approximately 24 hours. Scanning electron microscopy (SEM) electron backscatter diffraction (EBSD) measurements were carried out on a field-emission SEM at an accelerating voltage of 25 kV and beam current of 13 nA, with an EBSD step size of 0.5 μm .

Nanoindentation maps were acquired from 25 μm by 25 μm regions of the polished microscopy samples. Displacement controlled nanoindentation to a depth of 200 nm was carried out with a loading rate of 0.05 μm /s, maximum force of 200 mN, and the unloading rate was 10 μm /s. Indents were spaced 1 μm apart. No force was applied prior to indentation. The data was plotted using a natural neighbor (weighted average of multiple surrounding datapoints) scattered interpolant to illustrate the microstructural features between the datapoints in the nanoindentation map. The histograms however, are of the raw data.

The mini-tensile specimens were excised from simple cubic PBF-L cuboids as shown in Fig. 1c. The nominal gauge dimensions of the mini-tensile specimens were 5.08 mm long $\times$ 2.54 mm wide $\times$ 1.5 mm thick (Fig. 1d). The authors note that the specimen geometry was chosen to be consistent with the previous studies by Derimow et al. [22, 26]. Quasi-static uniaxial tensile testing was performed in the build direction (Z) at room temperature/air with a strain rate of $1 \times 10^{-3}\text{s}^{-1}$ up to failure using a servo-hydraulic load frame under displacement control. Strain was measured using a physical extensometer with gauge length of 3.0 mm. Eight replicates per condition were tested to failure.

3. Results and discussion

The microstructure of the $\text{Ti}|_{\text{H}_2+\text{G}1}$ and $\text{Ti}|_{\text{H}_2+\text{G}2}$ conditions are presented as EBSD maps in Fig. 2a–b, such that the coloring is shaded according to the aspect ratio of the α grains, where an aspect ratio of 1 represents a perfect circle and 0 would be a straight line. The coloring is overlaid onto the image quality of the EBSD maps. To highlight the microstructural changes resulting from the THRM process, a Ti-6Al-4V microstructure from previous work [27] that utilized blocks from this same build is shown in Fig. 2c, where this specimen was vacuum heat treated for 2 hours at 800 °C (stress-relieved). The lamellar $\alpha + \beta$ microstructure is typically what is observed when a PBF-L Ti-6Al-4V specimen is either stress-relieved or HIP'd [26], which has been drastically altered by the THRM process for $\text{Ti}|_{\text{H}_2+\text{G}1}$ and $\text{Ti}|_{\text{H}_2+\text{G}2}$ in Figs. 2a–b. The grain aspect ratio as obtained via EBSD is plotted with respect to the area fraction for all three microstructures in Fig. 2d, where there is a distinct shift towards an aspect ratio of 1 for the THRM specimens in this work relative to the stress-relieved condition. The globularization observed in this work is consistent with the microstructural observations by Dunstan et al. [15], as the same procedure was followed, thereby confirming and reinforcing the reproducibility of the THRM treatment. No distinct microstructural changes are observed between the $\text{Ti}|_{\text{H}_2+\text{G}1}$ and $\text{Ti}|_{\text{H}_2+\text{G}2}$ conditions, as the Ti_3Al precipitates are in the nanoscale regime [22], and would not be visible at this magnification.

Nanoindentation maps and histograms are presented for the $Ti|_{H_2+G1}$ (Fig. 3a–b) and $Ti|_{H_2+G2}$ (Fig. 3c–d) conditions. The nanoindentation maps display a 25 μm $\times$ 25 μm field-of-view (FOV), where the hardness intensity heatmap color scheme is represented as a histogram in Figs. 3b,d with the same coloring. The microstructures that are visible for the $Ti|_{H_2+G1}$ and $Ti|_{H_2+G2}$ conditions in Fig. 3a,c, respectively, show α grains with similar features, with bright spots indicated in yellow (highest intensity color) to represent the highest hardness regions. The authors note that FOVs for both conditions are arbitrary, and sampling may increase the visual presence of the highest intensity/harder grains. However, the histograms for the conditions quantitatively depict a decrease in lower hardness grains from the $Ti|_{H_2+G1}$ to the $Ti|_{H_2+G2}$ condition, with a shift towards grains with hardness values in the 5.5 GPa range, which is less likely due to FOV sampling as these intermediary values between low hardness and high hardness grains are more pronounced. Coincidentally, the amount of high hardness values is similar for both FOVs, allowing for a closer comparison of the hardness shift towards higher values in the $Ti|_{H_2+G2}$ condition relative to the $Ti|_{H_2+G1}$ condition, indirectly showing that the $Ti|_{H_2+G2}$ condition resulted in α_2 /Ti_3Al precipitation from the 100 hour aging.

In order to further investigate the mechanical properties, mini-tensile specimens were uniaxially tested in the exact same manner with the same sample geometry with respect to previous work from the present authors in Refs. [22, 26, 27]. The authors note, however, that the gauge length to width ratio in this work is 2:1, which is different than in the work by Dunstan et al. [15], where a ratio of 4:1 was utilized. Engineering stress-strain curves are shown in Fig. 4a–b, where the observed work-hardening behaviors are relatively similar. However, they appear elevated in strength for the $Ti|_{H_2+G2}$ condition, as highlighted in Fig. 4b. The mechanical properties for both conditions are summarized in Table 3. Analysis of variance (ANOVA) statistics were applied to both datasets to determine whether there were any statistically significant differences between the measured values. The values for modulus (E), uniform elongation (ε_u), and total elongation (ε_t) were calculated to have P values $>$ 0.05, implying that these values are not statistically different. Both yield (σ_{YS}) and ultimate tensile strength (σ_{UTS}) values, however, have P values $<$ 0.001, implying that they are statistically different, and can be reliably compared. The work by Dunstan et al. [15] demonstrated an increase in total elongation of the $Ti|_{H_2+G1}$ condition relative to the other temperatures and conditions tested in that work, due to the smaller parent-β grain size resulting from the 850 °C temperature (T_{max} in their work). The elongation in the present study cannot be directly compared due to the specimen geometry due to the differences in tensile geometry; however, these values are consistent with ε_t observations from from Derimow et al. [22] (approximately 30%) where the same geometry was used. The specimens in Ref. [22], however, had undergone HIP treatment at 920 °C , and therefore porosity was not a contributing failure mechanism. The similarity of ε_t values to previous work for specimens that have been HIP'd is consistent with the increased ductility observed by Dunstan et al. [15]. There was a small increase in the average σ_{YS} (+16 MPa) and σ_{UTS} (+12 MPa) values of the Ti$|_{\mathrm{H_2+G2}}$ condition relative to the Ti$|_{\mathrm{H_2+G1}}$ condition. This increase in strength is consistent with the α_2 precipitation hardening observed by Derimow et al. [22] for material from the exact same build, but subjected to a different starting heat treatment.

Table 3. Summary of tensile properties. σ_{YS} = yield strength, E = modulus, ε_u = uniform elongation, σ_{UTS} = ultimate tensile strength, ε_t = total elongation. Standard deviations (1σ) are presented next to the values. ANOVA = Analysis of Variance, where the P-values are such that values of $P > 0.05$ are considered to be not statistically different, while values of $P < 0.001$ are considered statistically significant.

Condition	Color	σ_{YS} (MPa)	E (GPa)	ε_u (%)	σ_{UTS} (MPa)	ε_t (%)
Ti$|_{\mathrm{H_2+G1}}$		846 ± 3	109 ± 2	11 ± 1	933 ± 3	32 ± 5
Ti$|_{\mathrm{H_2+G2}}$		862 ± 5	111 ± 15	11 ± 2	945 ± 4	30 ± 9
ANOVA	–	$P < 0.001$	$P > 0.05$	$P > 0.05$	$P < 0.001$	$P > 0.05$

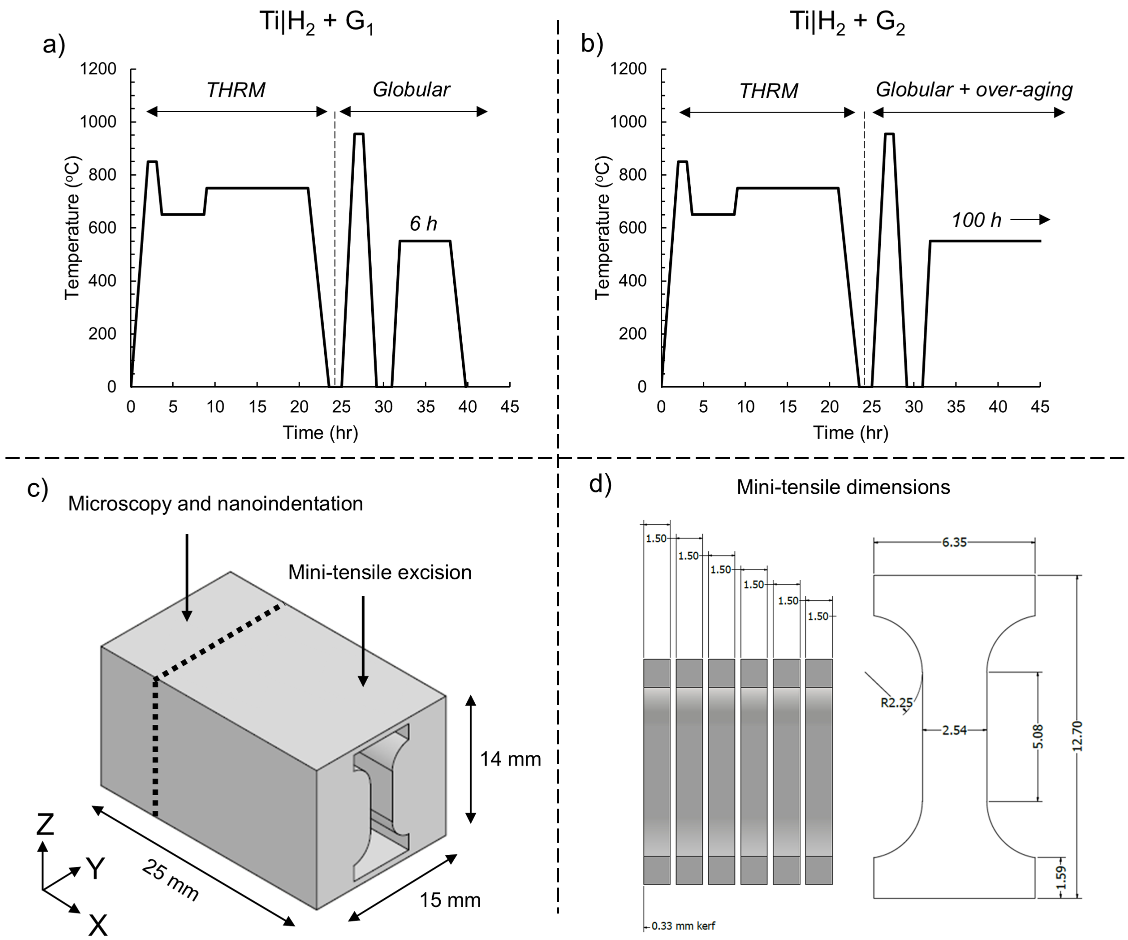

Fig. 1. a) Optimized THRM + Globularization treatment repeated from Ref. [15], referred to in this work at Ti$|_{H_2+G1}$. b) This same processing, however, with 100 h of aging instead of 6h, referred to in this work as Ti$|_{H_2+G2}$. c) PBF-L as-built block with nominal dimensions, and characterization and excision locations. d) Mini-tensile specimen geometry.

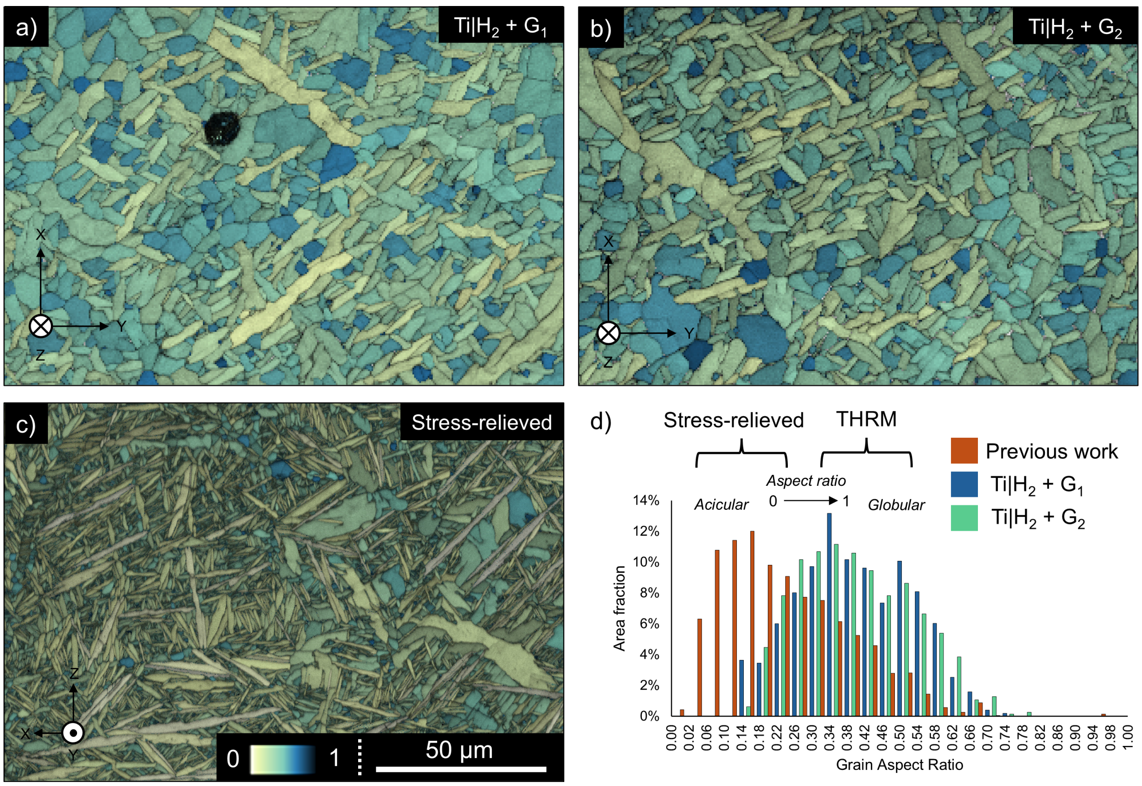

Fig. 2. EBSD aspect ratio map overlaid onto image quality for a) $Ti|_{H_2+G1}$, b) $Ti|_{H_2+G2}$, and c) an 800 °C stress-relief treatment stemming from the same build, however originating in previous work [27]. d) Grain aspect ratio plotted against area fraction for the field of view.

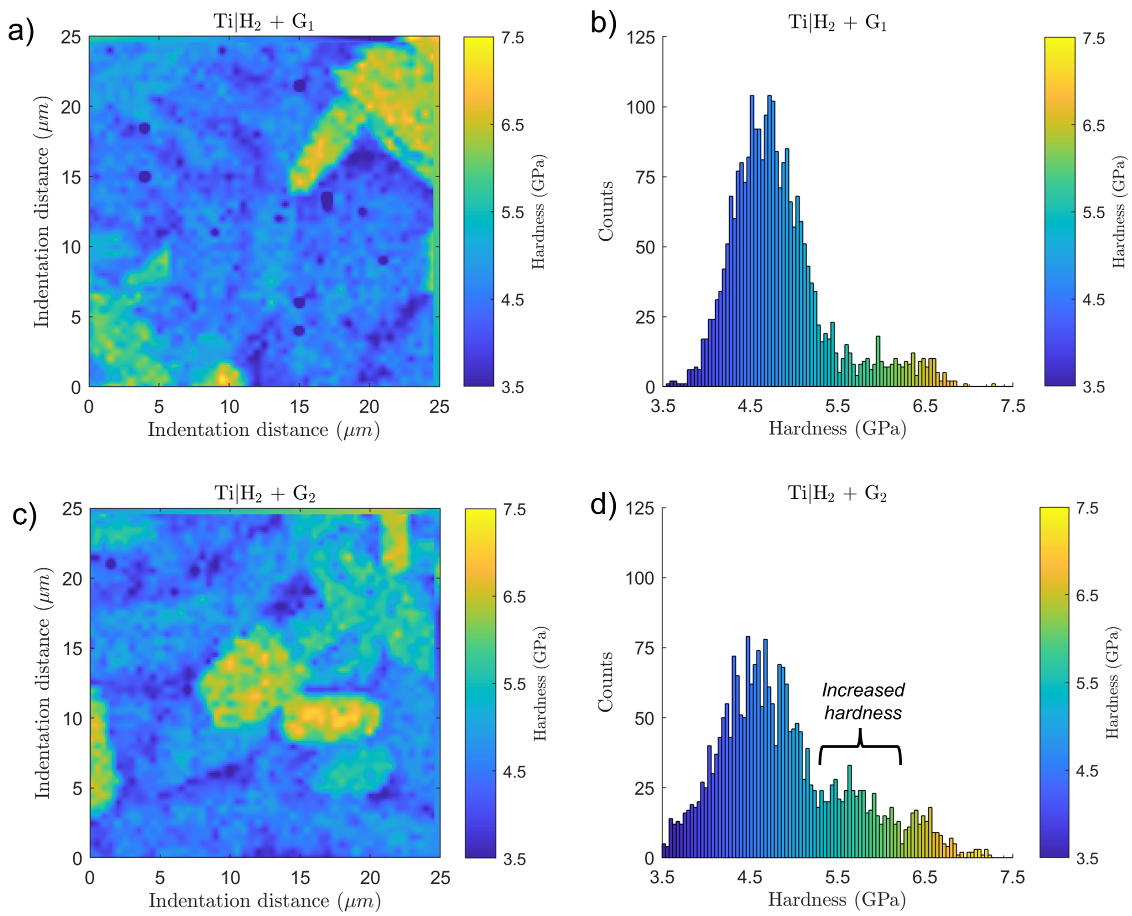

Fig. 3. a) Nanoindentation map of the Ti$|_{H_2+G1}$ condition, b) hardness histogram with the same heatmap color scheme. c) Nanoindentation map of the Ti$|_{H_2+G2}$ condition, d) hardness histogram with the same heatmap color scheme.

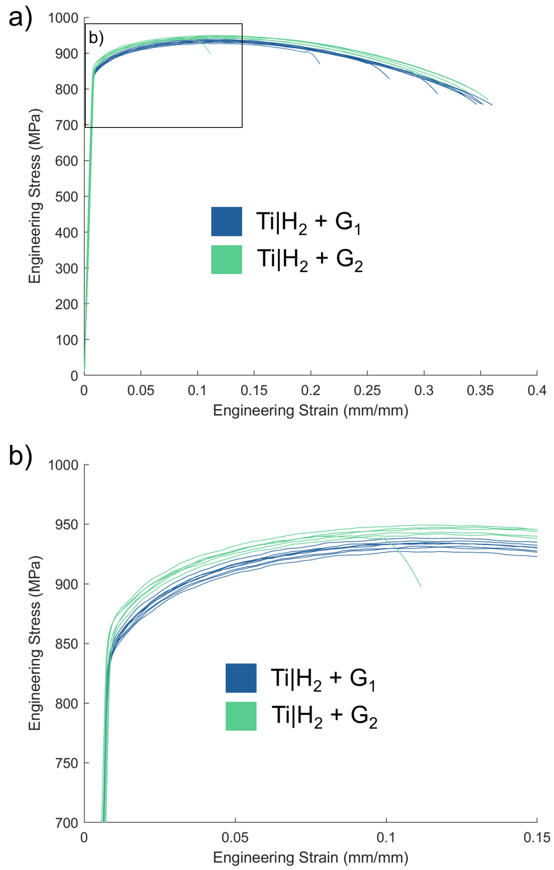

Fig. 4. Engineering stress-strain curves for the $\mathrm{Ti}|_{\mathrm{H_2+G1}}$ and $\mathrm{Ti}|_{\mathrm{H_2+G2}}$ condition, highlighting a reduced view in b) after yielding.

4. Summary

This work is a brief investigation into the viability of solution treatment and over-aging (STOA) as a post-processing step to improve the mechanical properties of PBF-L Ti-6Al-4V that has been subjected to a thermo-hydrogen refinement of microsctructure (THRM) treatment to promote globularization of the PBF-L Ti-6Al-4V α phase. The findings are highlighted below:

- The optimized THRM treatment from Dunstan et al. [15] was repeated for this work ($Ti|_{H_2+G1}$), utilizing material from previous studies by Derimow et al. [26, 27]. There was a a distinct shift in the microstructure towards globularization of the α laths, consistent with previous THRM-based investigations [13–15].
- Nanoindentation maps highlight a shift towards harder grains for the optimized THRM treatment that had extended the final step from 6 hours to 100 hours ($Ti|_{H_2+G2}$). This indicates precipitation hardening of the α grains via coherent Ti_3Al (α_2) particles, consistent with the observations by Derimow et al. [22].
- Mini-tensile testing resulted in a slight increase in yield and ultimate tensile strength for the over-aged condition, with no statistically significant differences observed in the modulus, uniform elongation, or total elongation. These results are also consistent with previous work [22].

While the tensile strength and hardness increases in this work are small, the observations are consistent with Ti_3Al precipitation hardening in Ti-6Al-4V alloys. This work serves as a proof-of-concept to further develop optimization studies to leverage both THRM and STOA techniques in a manner that can improve the mechanical properties of PBF-L Ti-6Al-4V with varying iterations of the times, temperatures, and pressures of the post-processing steps.

5. Declaration of competing interest

Brady Butler is a co-inventor of the patent, “Thermo-hydrogen refinement of microstructure of titanium materials.” U.S. Patent 11,624,105 [34]. The authors declare that they have no other competing financial interests or personal relationships that could have appeared to influence the work reported in this paper.

6. Acknowledgments

The authors wish to thank James Paramore and Matthew Dunstan for the helpful dialog regarding the feasibility of this work. This paper describes objective technical results and analysis. Any subjective views or opinions that might be expressed in the paper do not necessarily represent the views of the U.S. Department of Energy, U.S. Department of Commerce, or the United States Government. This work is supported by the Los Alamos National Laboratory Directed Research and Development (LDRD) Project 20230128DR.

[1] G. Lütjering, Influence of processing on microstructure and mechanical properties of $(\alpha + \beta)$ titanium alloys, Materials Science and Engineering A 243 (1-2) (1998) 32–45. doi:10.1016/s0921-5093(97)00778-8.
[2] P. G. Partridge, The crystallography and deformation modes of hexagonal close-packed metals, Metallurgical Reviews 12 (1) (1967) 169–194. doi:10.1179/mtlr.1967.12.1.169.
[3] I. Jones, W. Hutchinson, Stress-state dependence of slip in Titanium-6Al-4V and other H.C.P. metals, Acta Metallurgica 29 (6) (1981) 951–968. doi:10.1016/0001-6160(81)90049-3.
[4] S. Zaefferer, A study of active deformation systems in titanium alloys: Dependence on alloy composition and correlation with deformation texture, Materials Science and Engineering: A 344 (1-2) (2003) 20–30. doi:10.1016/S0921-5093(02)00421-5.
[5] W. Burgers, On the process of transition of the cubic-body-centered modification into the hexagonal-close-packed modification of zirconium, Physica 1 (7-12) (1934) 561–586. doi:10.1016/S0031-8914(34)80244-3.
[6] C. A. Stubbington, A. W. Bowen, Improvements in the fatigue strength of Ti-6Al-4V through microstructure control, J Mater Sci 9 (6) (1974) 941–947. doi:10.1007/BF00570387.
[7] T. Ahmed, H. J. Rack, Phase transformations during cooling in α+β titanium alloys, Materials Science and Engineering A 243 (1-2) (1998) 206–211. doi:10.1016/S0921-5093(97)00802-2.
[8] J. Yang, H. Yu, J. Yin, M. Gao, Z. Wang, X. Zeng, Formation and control of martensite in Ti-6Al-4V alloy produced by selective laser melting, Materials & Design 108 (2016) 308–318. doi:10.1016/j.matdes.2016.06.117.
[9] W. Xu, M. Brandt, S. Sun, J. Elambasseril, Q. Liu, K. Latham, K. Xia, M. Qian, Additive manufacturing of strong and ductile Ti-6Al-4V by selective laser melting via in situ martensite decomposition, Acta Materialia 85 (2015) 74–84. doi:10.1016/j.actamat.2014.11.028.
[10] S. Cao, R. Chu, X. Zhou, K. Yang, Q. Jia, C. V. S. Lim, A. Huang, X. Wu, Role of martensite decomposition in tensile properties of selective laser melted Ti-6Al-4V, Journal of Alloys and Compounds 744 (2018) 357–363. doi:10.1016/j.jallcom.2018.02.111.
[11] S. Semiatin, V. Seetharaman, I. Weiss, Flow behavior and globularization kinetics during hot working of Ti–6Al–4V with a colony alpha microstructure, Materials Science and Engineering: A 263 (2) (1999) 257–271. doi:10.1016/S0921-5093(98)01156-3.
[12] R. Wood, The Effect of Variables on the Fatigue Behavior of Ti-6Al-4V, Topical Report CS-2934, Battelle Columbus Laboratories (1984).
URL https://www.epri.com/research/products/CS-2934
[13] J. D. Paramore, Z. Z. Fang, M. Dunstan, P. Sun, B. G. Butler, Hydrogen-enabled microstructure and fatigue strength engineering of titanium alloys, Sci Rep 7 (1) (2017) 41444. doi:10.1038/srep41444.

[14] M. Knezevic, S. Ghorbanpour, N. C. Ferreri, I. A. Riyad, A. D. Kudzal, J. D. Paramore, S. C. Vogel, B. A. McWilliams, Thermo-hydrogen refinement of microstructure to improve mechanical properties of Ti–6Al–4V fabricated via laser powder bed fusion, Materials Science and Engineering: A 809 (2021) 140980. doi:10.1016/j.msea.2021.140980.

[15] M. K. Dunstan, M. O. Vaughn, J. D. Paramore, B. G. Butler, A. D. Kudzal, K. J. Hemker, Optimization of microstructural manipulation and ductility in laser powder bed fusion Ti-6Al-4V through hydrogen heat treatments, Materials Science and Engineering: A 873 (2023) 145061. doi:10.1016/j.msea.2023.145061.

[16] G. Welsch, G. Lutjering, K. Gazioglu, W. Bunk, Deformation Characteristics of Age Hardened Ti-6Al-4V, Metallurgical Transactions A 8A (January) (1977) 169–177.

[17] A. Gysler, G. Lütjering, Influence of test temperature and microstructure on the tensile properties of titanium alloys, Metall Trans A 13 (8) (1982) 1435–1443. doi:10.1007/BF02642882.

[18] T. K. G. Namboodhiri, C. J. McMahon, H. Herman, Decomposition of the a-Phase in Titanium-Rich Ti-Al Alloys, METALLURGICAL TRANSACTIONS 4 (1973) 1323–1331.

[19] D.-G. Lee, S. Lee, C. S. Lee, Quasi-static and dynamic deformation behavior of Ti–6Al–4V alloy containing fine α2-Ti3Al precipitates, Materials Science and Engineering: A 366 (1) (2004) 25–37. doi:10.1016/j.msea.2003.08.061.

[20] D.-G. Lee, S. Lee, Effects of nano-sized α2 (Ti3Al) particles on quasi-static and dynamic deformation behavior of Ti-6Al-4V alloy with bimodal microstructure, J Mater Sci 40 (15) (2005) 4077–4084. doi:10.1007/s10853-005-1914-y.

[21] E. Cerri, E. Ghio, S. Spigarelli, M. Cabibbo, G. Bolelli, Static and dynamic precipitation phenomena in laser powder bed-fused Ti6Al4V alloy, Materials Science and Engineering: A 880 (2023) 145315. doi:10.1016/j.msea.2023.145315.

[22] N. Derimow, J. T. Benzing, J. Garcia, Z. S. Levin, P. Lu, N. Moser, C. Beamer, F. W. DelRio, N. Hrabe, Precipitation hardening of laser powder bed fusion Ti-6Al-4V, Materials Science and Engineering: A 921 (2025) 147549. doi:10.1016/j.msea.2024.147549.

[23] A. Radecka, J. Coakley, V. Vorontsov, T. Martin, P. Bagot, M. Moody, D. Rugg, D. Dye, Precipitation of the ordered α2 phase in a near-α titanium alloy, Scripta Materialia 117 (2016) 81–85. doi:10.1016/j.scriptamat.2016.02.015.

[24] A. Radecka, P. Bagot, T. Martin, J. Coakley, V. Vorontsov, M. Moody, H. Ishii, D. Rugg, D. Dye, The formation of ordered clusters in Ti–7Al and Ti–6Al–4V, Acta Materialia 112 (2016) 141–149. doi:10.1016/j.actamat.2016.03.080.

[25] ISO 13485:2016, Medical devices — Quality management systems — Requirements for regulatory purposes, ISO Standards (2016).
URL https://www.iso.org/standard/59752.html

[26] N. Derimow, J. T. Benzing, H. Joress, A. McDannald, P. Lu, F. W. DelRio, N. Moser, M. J. Connolly, A. I. Saville, O. L. Kafka, C. Beamer, R. Fishel, S. Sarker, C. Hadley, N. Hrabe, Microstructure and mechanical properties of laser powder bed fusion Ti-6Al-4V after HIP treatments with varied temperatures and cooling rates, Materials & Design 247 (2024) 113388. doi:10.1016/j.matdes.2024.113388.

[27] N. Derimow, High Pressure Heat Treatment Development for Laser Powder Bed Fusion Ti-6Al-4V Alloy: Observations and Findings, NIST Internal Report NIST IR 8551 (2024). doi:10.6028/NIST.IR.8551.

[28] ISO 17025, General requirements for the competence of testing and calibration laboratories, ISO Standards (Revised in 2017) (2005).

[29] ASTM E2823, Test Method for Analysis of Nickel Alloys by Inductively Coupled Plasma Mass Spectrometry (Performance-Based Method), ASTM Standards (2017). doi:10.1520/E2823-17.

[30] ASTM E1409-13, Standard Test Method for Determination of Oxygen and Nitrogen in Titanium and Titanium Alloys by Inert Gas Fusion, ASTM Standards (2013). doi:10.1520/E1409.

[31] ASTM E1447-09, Standard Test Method for Determination of Hydrogen in Titanium and Titanium Alloys by Inert Gas Fusion Thermal Conductivity / Infrared Detection, ASTM Standards ((Reapproved 2016)) (2009). doi:10.1520/E1447-09R16.

[32] ASTM E1941-10, Standard Test Method for Determination of Carbon in Refractory and Reactive Metals, ASTM Standards (2016). doi:10.1520/E1941-10.

[33] ASTM F3001-14, Standard Specification for Additive Manufacturng Titanium-6 Aluminum-4 Vanadium ELI (Extra Low Interstitial) with Powder Bed Fusion, ASTM Standards (2014) 1–6doi:10.1520/F3001-14.

[34] J. D. Paramore, B. G. Butler, M. K. Dunstan, J. P. Ligda, Z. Z. Fang, Thermo-hydrogen refinement of microstructure of titanium materials. (Nov. 2023).
URL https://ppubs.uspto.gov/api/patents/html/11624105?source=USPAT&requestToken=eyJzdWIiOiJmNTEwOWM5Zi0xMDE5LTQ1ZDQtYjY1Yi01OWMwZDQ0YzQyODgiLCJ2ZXIiOiI2YTBjODIyZC0wMWM1LTRkMTMtYjVjNi04Njg5ZGRmZTc2YzgiLCJleHAiOjB9